Applied Thermal Engineering, Volume 180, November 2020, Article number 115869
DOI: 10.1016/j.applthermaleng.2020.115869

Gas Turbine Minimum Environmental Load Extension with Compressed Air Extraction for Storage

[1]Kamal Abudu **[1*]Uyioghosa Igie** **[2]Orlando Minervino** **[2]Richard Hamilton**

[1]School of Aerospace, Transport and Manufacturing
Cranfield University
Cranfield, Bedfordshire, MK43 0AL
United Kingdom
*Email: u.igie@cranfield.ac.uk

[2]Mitsubishi Hitachi Power Systems Europe
The Point, 37 North Wharf Road
London, W2 1AF
United Kingdom

ABSTRACT

The fact that most renewable forms of energy are not available on-demand and are typically characterised by intermittent generation currently makes gas turbine engines an important source of back-up power. This study focuses on one of the capabilities that ensure that gas turbines are more flexible on the electric power grid. The capability here is the minimum environmental load that makes it possible to keep a gas turbine engine on the grid without a shut-down, to offer grid stability, adding inertia to the grid in periods when there is no demand for peak power from the engine. It is then desirable to operate the engine at the lowest possible load, without infringing on carbon monoxide emissions that becomes dominant. This paper demonstrates this potential through the extraction of the pressurised air from the back end of the compressor into an assumed energy storage system. The simulation of the engine performance using an in-house tool shows the additional reduction of the power output when the maximum closing of variable inlet guide vane is complemented with air extractions. However, the identified key strategy for achieving a lower environmental load (with same carbon monoxide emission limit) is to always maintain the design flame temperature. This is contrary to the conventional approach that involves a decrease in such temperatures. Here, a 34% reduction in load was achieved with 24% of flow extraction. This is shown to vary with ambient temperatures, in favour of lower temperatures when the combustor inlet pressures are higher. The emission models applied were based on empirical correlations and shows that higher combustor inlet pressures, high but constant flame temperatures with core flow reduction is crucial to obtaining a low environmentally compliant load. The compressor analysis shows that choking is a noticeable effect at a higher rate of extractions; this is found to occur at the stages closest to the extraction location.

Keywords: flexibility, gas turbine, turndown, emissions

1. INTRODUCTION

Environmental impact has brought about measures to curb air pollution from fossil fuels. The increasing adoption of renewable energy to address these concerns means that fossil-fuelled combustion engines must be more environmentally friendly and operate flexibly in the emerging European energy mix. Natural gas-fired stationary gas turbines in combined cycle operation outperform coal-fired power plant in terms of CO_2 emissions and thermal efficiency for the same amount of power generated [1]. The prioritization of renewables in some countries now means that a conventional power plant has to operate more flexibly with wind and solar power. For gas turbines (GTs), operational flexibility is also described as the ease with which an engine copes with varying power demand that is linked to the intermittency of renewable power. According to Bistline [2], a few yardsticks determine GT operational flexibility; these are: ramp rate, minimum runtimes, part-load efficiency, and minimum turndown (emissions-compliant or minimum environmental load – MEL). For MEL, the criterion is described by the minimum power output a GT operates without infringing on emissions (particularly CO) or combustor stability limits. **Table 1** shows the current limits of CO and NO_x pollutant for existing gas turbines operated in Europe. This indicates that the yearly averaged emission of CO and NO_x should not exceed 50mg/Nm^3 for existing gas turbines in continuous operation. Additionally, the daily averaged NO_x emission is capped at 55mg/Nm^3. These limits are specified in the Best Available Technique (BAT) reference document (BREF) for large combustion plants [3]. Low load operations exist at periods of low power demand. This operation is characterized by an increase in CO, as a result of incomplete combustion which occurs when there is a reduced supply of oxygen (air mass flow). Reducing power output at the off-peak period has also been found more beneficial than a complete shutdown of the machine. This is primarily because every start-up of the engine consumes life in terms of thermo-mechanical fatigue.

For GTs, it is desirable to reduce the low load capability without exceeding the CO limits. This can be made possible by some approaches that include Variable Inlet Guide Vane (VIGV) extension [4], use of bleed-off valves (BOV) [5] and through bleed extraction for storage (Compressed Air Energy Storage – CAES) that applies to this study. Pratyush et al. [6] in a Siemens study indicated that extended VIGV closure, bypassing compressed air around the combustor, and optimizing rotor cooling can bring about a MEL of 40% and 28% (without and with catalytic CO capturing respectively). Similarly, Alstom explored the use of sequential burners in their GT26, currently owned by Ansaldo Energia; Ruchti et al. [7] suggest that the engine could achieve a MEL of 20% by switching off one of its burners and still operate satisfactorily in combined cycle operation. More recently, Ansaldo Energia investigated the use of BOV, presented in Coiffi et al. [5]. The authors performed a thermodynamic and aerodynamic analysis of a BOV, showing a 29% reduction of MEL. In addition to other modifications presented in Malavasi et al. [8], it can be reduced further. The article highlights the trade-off between low load operation and efficiency penalty and suggests consideration before implementation. Other methods to

reduce MEL such as the use of preheaters to decrease compressor inlet flow and using auto thermal syngas generators to facilitate complete combustion are highlighted in Eberhard et al. [9] and Max et al. [10] respectively.

Huntorf and Macintosh plants in Germany and the USA respectively, are examples of the successful application of CAES technology. These systems operate similar to a gas turbine without a continuous connecting shaft between the compressor and the turbine. This type of configuration has inspired several research studies that investigate a variation of the turbomachinery arrangements. Nevertheless, the issue of MEL does not arise, as the flow extraction does not occur with the combustor in operation; as the compressor is driven by an electric motor. Thus, the configuration is likely to pose less constraint on how much flow can be extracted from the compressor. The practical application of CAES flow extraction from conventional gas turbine configuration does not currently exist. Very few studies have investigated this and includes works of Wojcik and Wang *[11]* and Parsons Brinckerhoff *[12]*. The former explores the feasibility of integrating adiabatic CAES systems with a combined cycle gas turbine (CCGT). Their proposed configuration uses the gas turbine compressor for first stage CAES compression, adding: additional compressors, intercoolers, aftercoolers, a thermal energy store and air expanders. For air extraction, the bottoming cycle is still in operation, amounting to a total low load of 20% in CCGT operation. This study does not consider MEL (that is concerning CO emissions) when there is a reduced airflow and thus power output. Ref *[12]* only presents a technical review of the potentials of extraction for MEL and not the methodology of the analysis. The stand-alone GT is the focus of Igie et al. *[13]* that investigates the impact of flow extractions at 3 consecutive rear stage locations, using a single-shaft engine model of 10 compressor stages. The study was conducted at full load extraction and reports that extracting after the last stage proved safer with regards to surge margins of the compressor. It also adds that it is the most suitable location if heat storage is considered - related to the higher temperatures and pressures when compared to other parts of the compressor. Other analyses on interstage flow extractions in the study were shown to cause the stage to move towards choke, but subsequent stages towards stall. This behaviour is also highlighted for a two-shaft engine with power turbine, in the work of Hackney et al *[14]*. Similarly, Yang et al. *[15]* demonstrate the impact of air extraction (up to 30%) at the end of the compressor, keeping the exhaust gas temperature constant. The purpose of the study was to improve the system efficiency and flexibility for combined cooling, heating and power plant at deep-peak load. Conversely, the flexibility explored here relates to gas turbine off-peak periods in which renewable power generation is high or generally low demand for power.

The published MEL values shown in **Figure 1** are indicative values of different engine manufacturers. These have been achieved by different technological modifications and in one case, with a different combustor design – sequential combustion. The figure also shows that the average MEL value is about

49%, while the highest and lowest being at 75% and 25% respectively. Currently, no engine-level analysis on air extraction or CAES has addressed the potential MEL extension as shown in the present study. Further to this, the work here demonstrates a realistic rated MEL comparable to those presented in **Figure 1** and based on the emissions limit in **Table 1**. For the extended MEL, a novel approach has been deployed by the combinations of VIGV closure, air extractions and maintaining the combustor mean temperature as the control constraint. Other contributions of the papers include the analysis of the influence of ambient conditions on extended MEL and the potential of another turndown scheme. The main cases investigated include the following:

1. Effect of varied flow extraction at design point (DP) with maximum VIGV opening
2. Identification of the design MEL using VIGV closure and subsequent drop in combustor mean temperature (CMT) or flame temperature.
3. MEL extension through VIGV closure and air extraction, while keeping the CMT constant during the turndown phases.

Table 1: Maximum BAT-associated emission level for NOx and CO *[3]*

NOx emission limits (BREF)- Max	**(mg/Nm^3)**	**ppmv**
Existing OCGT plants (yearly average)	50	26.2
INDICATIVE- CO emission limits (BREF)- Max		
Existing OCGT plants (yearly average)	50	40.5

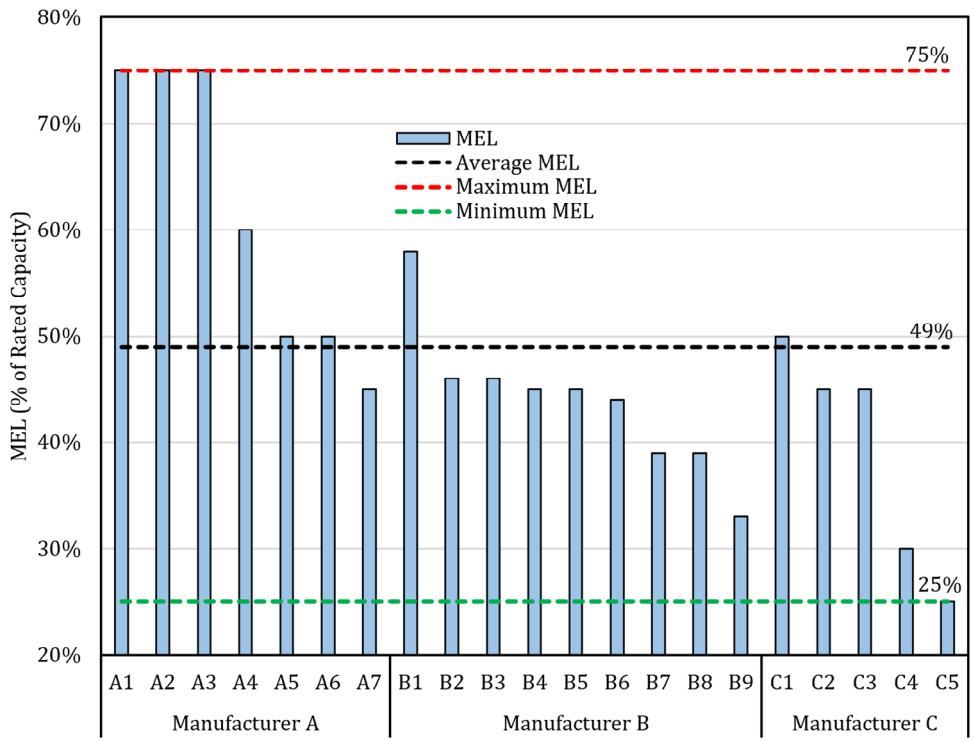

Figure 1: MEL of different engines [16-36]

2. ENGINE MODEL – METHOD

The gas turbine performance is modelled and simulated using Turbomatch, Cranfield University's in-house software. It is a zero-dimensional code in FORTRAN language, which is used for steady-state and transient gas turbine simulations. The tool employs a modified Newton-Raphson method to achieve convergence. It approximates turbomachinery effects in the compressor and turbine, using standard maps that are scaled to match the user-defined parameters. This is achieved by using scaling factor (SF) of specified parameters such as pressure ratio (PR), component isentropic efficiency (η_{is}) and corrected mass flow (CMF) as shown in **Equation 1** to **3**. The denominator in these equations is the original values of the standard map, while the numerator is the new specified values. Similarly, *DPmap* refers to the standard map and DP is the design point of the model. For the CMF, the correction of the actual mass flow is made with reference to sea level condition as shown in **Equation 4**. In addition, the embedded generalized combustor map is used to estimate the variations in combustor efficiency and pressure drop.

$$SF_{PR} = \frac{PR_{DP} - 1}{PR_{DPMap} - 1} \qquad \textbf{Equation 1}$$

$$SF_{\eta is} = \frac{\eta_{isDP}}{\eta_{isDPMap}} \qquad \textbf{Equation 2}$$

$$SF_{CMF} = \frac{CMF_{Dp}}{CMF_{DPMap}} \qquad \textbf{Equation 3}$$

Where

$$CMF = \dot{m}_{in} \cdot \frac{101325Pa}{P_{in}} \cdot \sqrt{\frac{T_{in}}{288.15K}} \qquad \textbf{Equation 4}$$

For design and off-design computations, the software performs the calculations that must satisfy the compatibility of work, mass flow, and shaft speed as indicated in **Equation 5 to 7** respectively. The implication of this for **Equation 6** is that the term on the left-hand side (non-dimensional mass flow of turbine inlet) is approximately constant. This is achieved by varying the terms on the right hand side of the equation. On the side of the equation, the inverse of the pressure ratio and the turbine temperature ratio (the second and fourth term) vary more significantly than the other terms.

$$\mathrm{PO} = \dot{m}_{17} \cdot c_{p_{17}} \cdot (T_{17} - T_{21}) - \dot{\mathrm{m}}_2 \cdot c_{\mathrm{p}_2} \cdot (\mathrm{T}_9 - \mathrm{T}_2) \qquad \textbf{Equation 5}$$

$$\frac{\dot{m}_{17}\sqrt{T_{17}}}{\mathrm{P}_{17}} = \frac{\dot{m}_2\sqrt{T_2}}{\mathrm{P}_2} \cdot \frac{\mathrm{P}_2}{\mathrm{P}_9} \cdot \frac{\mathrm{P}_9}{\mathrm{P}_{17}} \cdot \sqrt{\frac{\mathrm{T}_{17}}{\mathrm{T}_2}} \cdot \frac{\dot{m}_{17}}{\dot{m}_2} \qquad \textbf{Equation 6}$$

$$\frac{N}{\sqrt{T_{out}}} = \frac{N}{\sqrt{T_{in}}} \cdot \frac{\sqrt{T_{in}}}{\sqrt{T_{out}}}$$ **Equation 7**

Operational requirements can be attained by modulating the VIGV, which is accomplished through further scaling of component maps. Furthermore, models generated can be controlled using shaft speed, combustor outlet temperature (COT) or fixed power output. The CMT and exhaust gas temperature (EGT) can also be improvised as control constraints [33].

The heavy-duty gas turbine selected for this study is inspired by a generic Mitsubishi F-class engine. This class of engines is chosen as it constitutes a high percentage of the operating fleet of most OEMs. The single shaft, 185MW gas turbine, operates on natural gas and consists of 16 compression stages, a premixed low NOx combustor, a four-stage turbine and variable inlet guide vanes (VIGV). This engine type also features compressor inter-stage bleeds and a separate combustor bypass for the transition piece [16]. **Figure 2** is a schematic illustrating the engine model configuration and interconnections, which accounts for additional turbine cooling using compressor interstage bleeds. The interstage bleed is possible, given that the compressor is modelled as four bulk sections (and not individual stages). The figure also shows a bypass channel from the compressor exit to the combustor transition piece. It is crucial to note that the amount of bypass flow is a function of the load variation; this is similar to the schedule presented in Katsunori et al [34]. Thus, the turbine entry temperature (TET) is reduced further by the cooler bypass flow.

The specified DP performance at which the engine is modelled is indicated in **Table 2.** These are typical values that are either assumed based on the technology of the engine or from published data. The calculated design point parameters are presented in

Table *3*. These parameters are shown to be very close to the OEM published data with a maximum percentage error of 1%. In addition to the DP verification, the off-design performance of the model is compared to that of publicly available OEM data in **Figure A.1** of the Appendix. It shows the effect of ambient temperature variations on the power output, heat rate and exhaust flow for the model and reference engine. As can be observed, the differences are mostly negligible and are attributed to the component maps that is not identical to the OEM proprietary maps.

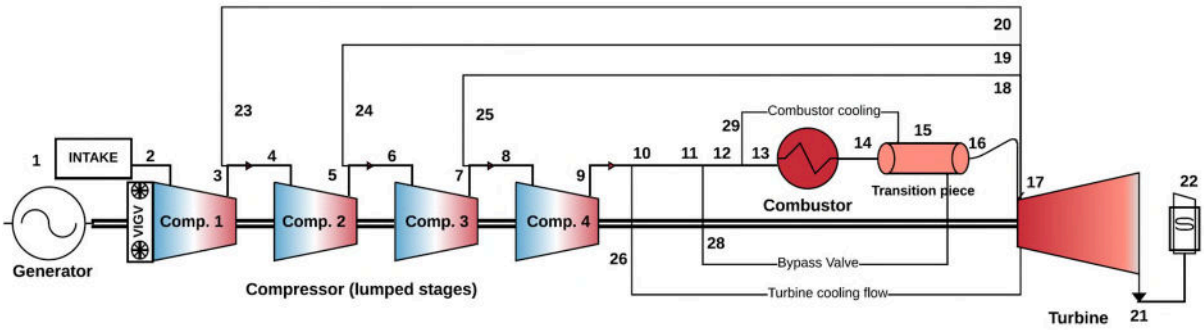

Figure 2: Engine schematic illustrating the interconnection of components

Table 2: Engine model DP and performance specification

Design Parameters		Comment
Ambient conditions	ISO	-
Intake mass flow	457kg/s	Ref [16]
Compressor overall pressure ratio	16	Ref [16]
Compressor overall efficiency	86%	assumed
Combustor pressure loss	4%	Ref [35]
Combustor efficiency	99%	assumed
Turbine efficiency	89%	assumed
Combustor mean temperature	1786K	Ref [36]
Fuel lower heating value	45.5MJ/kg	assumed

Table 3: DP performance – calculated parameters and % error

Performance Parameters	OEM Data	Model	%Error
Net power output	185.4MW	185.4MW	0.0%
Thermal efficiency	37.0%	37.0%	0.1%
Exhaust gas temperature	886.0K	895.3K	1.0%
Exhaust mass flow	468kg/s	468kg/s	0.0%

The compressor air extraction occurs at station 10 that is immediately after the bleed for the turbine cooling, indicated in **Figure A.2.** The air storage system depicted in the figure is only included for illustrative purposes and not modelled in this study; therefore, the gas turbine is treated as a standalone. The compressed air for storage is bled into the virtual tank, thereby reducing the engine model mass flow and moving the operating point of the compressor away from surge. The proximity to surge has been described as the surge margin utilisation (SMU), as defined by **Equation 8**. Assumed SMU value of 85% (i.e. 15% surge margin) is specified for the compressors at the design point.

Equation 8

$$SMU\ (\%) = \left(\frac{PR_{working} - PR_{min}}{PR_{stall} - PR_{min}}\right) \times 100$$

3. EMISSIONS MODEL – METHOD

The results from the performance simulation allow for the emission estimation through the calculated combustor flame temperature. Gulder [37] proposes a method to evaluate the primary zone temperature of a combustor using engine performance data and some constants. The parameters required include the combustor equivalence ratio, normalized fuel temperatures and pressures, and hydrogen to carbon (H/C) atomic ratio of fuel. For simplification, a global equivalence ratio is evaluated for the combustor that combines the pilot and main injector fuel to air ratios. In addition, the fuel is introduced at an assumed temperature and pressure identical to the compressor discharge with a H/C ratio of methane (CH_4) specified**. Equation 9.0-9.6** present the relations between the engine performance parameters and the flame temperature.

$$T_{flame} = A \cdot \sigma^{\alpha} \cdot \exp[\beta(\sigma + \lambda)^2] \cdot \pi^x \cdot \theta^y \cdot \psi^z \quad \textbf{Equation 9.0}$$

$$x = a_1 + b_1\sigma + c_1\sigma^2 \quad \textbf{Equation 9.1}$$

$$y = a_2 + b_2\sigma + c_2\sigma^2 \quad \textbf{Equation 9.2}$$

$$z = a_3 + b_3\sigma + c_3\sigma^2 \quad \textbf{Equation 9.3}$$

$$\pi = \frac{P_{fuel}}{P_{ambient}} \quad \textbf{Equation 9.4}$$

$$\theta = \frac{T_{fuel}}{T_{ambient}} \quad \textbf{Equation 9.5}$$

$$\psi = \frac{H}{C}\ atomic\ ratio\ of\ fuel \quad \textbf{Equation 9.6}$$

T_{flame}, σ, π, θ, ψ are primary zone flame temperature, equivalence ratio, normalized fuel pressure, normalized fuel temperature, and H/C atomic ratio of fuel respectively. A, α, β, λ, a_i, b_i, and c_i are constants with their values presented in **Table A1** of **Appendix A.** Further description of the flame temperature estimation is provided in the referred study.

The evaluated flame temperature is used to estimate the carbon monoxide (CO) emission using an empirical correlation for total combustor emissions presented in Rizk and Mongia [38]. Other proposed methods in the study require detailed combustor data that is not available from the performance model. **Equation 10** presents a modified correlation from the referred paper which estimates CO emissions.

$$CO(g/kg) = \frac{0.179 \times 10^9 \times \exp\left(\frac{7800}{T_{flame}}\right)}{\left[{P_{13}}^2 \times 10^3 \times (\tau - 0.4\tau_{ev}) \times \left(\frac{\Delta P_{13}}{P_{13}}\right)^{0.5}\right]} \quad \textbf{Equation 10}$$

In the equation, subscript 13 represents the combustor inlet station (w.r.t. **Figure 1**), while τ symbolizes the residence time. τ_{ev} which is the residence time of evaporation is assumed 0 as the fuel is in gaseous form. The primary zone residence times and liner pressure drop are assumed based on estimates from Etemad [39] and Lefebvre and Ballal [40].

Sullivan [41] proposes the NOx emissions model as presented in **Equation 11**. The correlation was derived from the evaluation of seven other studies on estimating NOx. The author demonstrates the validity of the correlation by computing a combustor geometry parameter (A_{Nox}) and identifying it as a constant. The value of A_{Nox} gives an indication of the residence time, which is usually required for detailed NOx estimation. The constant is evaluated as 0.554 (for the specific case considered) through the matching of predicted and published NOx emissions data at DP ISO operation [16]. The combustor inlet pressure, temperature, airflow and fuel-air ratio are also used in the estimation.

$$NO_x(ppmv) = A_{Nox} \times P_{13}^{0.5} \cdot f^{1.4} \cdot \dot{m}_9^{-0.22} \cdot \exp(T_{13}/250) \qquad \textbf{Equation 11}$$

4. ENGINE CONTROL STRATEGIES AND CASES

The engine schematic with an emphasis on the combustor temperatures (T_{flame}, CMT, COT and TET) is shown in **Figure A.2** of **Appendix A.** It can be noted from the previous discussions, that CMT is used as a control constraint in the simulations. All but the T_{flame} is obtained from the engine model. The control strategies for the respective cases investigated are shown in

Figure *3*, where rows A, B and C relates to Sections 5, 6 and 7 respectively. Section 5 study provides a basic understanding of flow extraction that can be directly compared with Igie et al [13] and Yang et al. [15], while Section 6 approach is comparable to Munoz de Escalona et al. [42] that did not account for emissions limit. Section 7 is related to the work of Therkorn et al [43] with a sequential combustor that involves keeping the first chamber temperatures entirely fixed, however, does not include any air extraction.

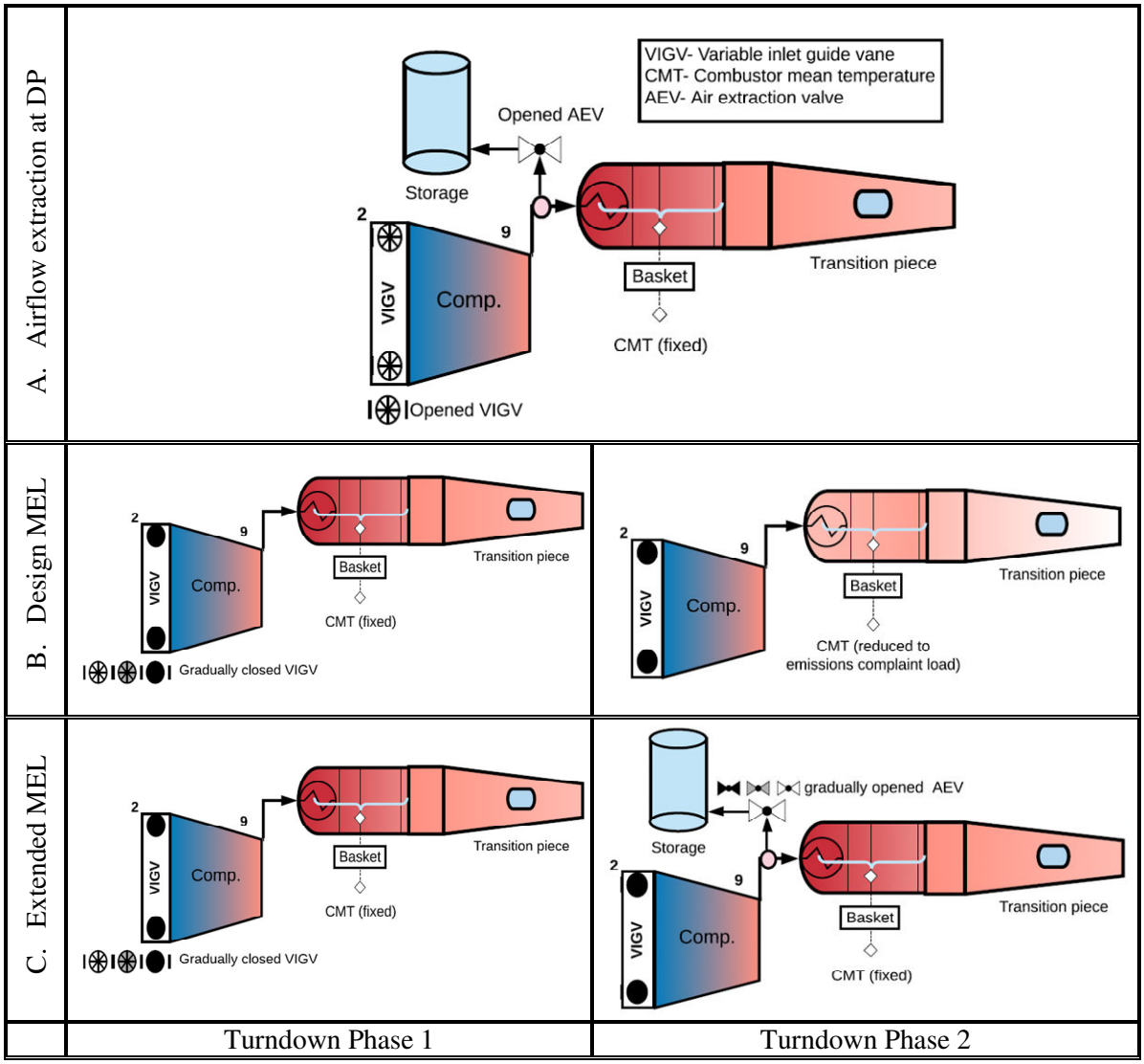

Figure 3: Engine control strategies related to the cases investigated

5. EFFECT OF FLOW EXTRACTION AT DP - MAXIMUM VIGV OPENING

As a precursor, the effect of flow extraction at full load and a constant CMT is presented in this section. The set-up of this simulation is illustrated in

Figure *3*A, which shows the extraction location behind the compressor discharge. The flow is extracted to a dummy storage, as a percentage of air flowing through station 10, and the quantity of air extracted is limited to 15%. The effect of the flow extraction is a drop in the pressure at the exit of the compressor, that brings about a drop in the overall pressure ratio (OPR) shown in **Figure 4**. There is also a drop in the compressor discharge temperature (CDT), arising from the reduced compressor work caused by mass flow reduction. These reductions bring about a decrease in the power output as shown in **Figure 5**. As the transition piece bypass cooling flow increases with lower power outputs for this engine type, the TET reduces further with more air extraction. The lower OPR of the compressor also translates to

lesser turbine inlet pressure that usually causes less expansion in the turbine section. However, this does not bring about a rise in EGT, due to a drop in the TET. The drop in TET provides potential life extension benefits for the turbine blades, although the EGT reduction can affect steam quality in CCGT operation. As for the power output change mentioned, the decline is primarily attributed to the reduced compressed airflow that is accompanied by a drop in the fuel flow. However, the decrease in fuel flow is necessary to maintain constant CMT. From **Figure 5**, it can also be observed that the fuel flow drops at a lower magnitude than the power output, resulting in lower thermal efficiency. There is a consistent reduction to all the parameters as the extracted flow increases from 5 to 15%.

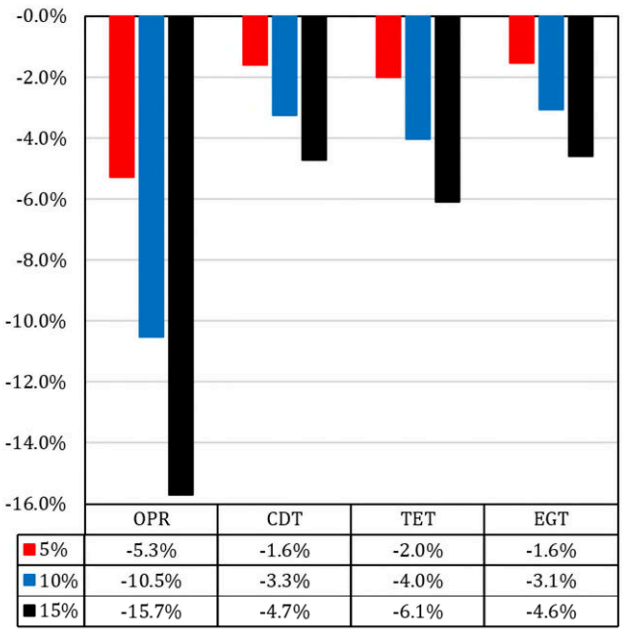

	OPR	CDT	TET	EGT
5%	-5.3%	-1.6%	-2.0%	-1.6%
10%	-10.5%	-3.3%	-4.0%	-3.1%
15%	-15.7%	-4.7%	-6.1%	-4.6%

Figure 4: Effect of flow extraction on OPR and temperatures – max VIGV opening

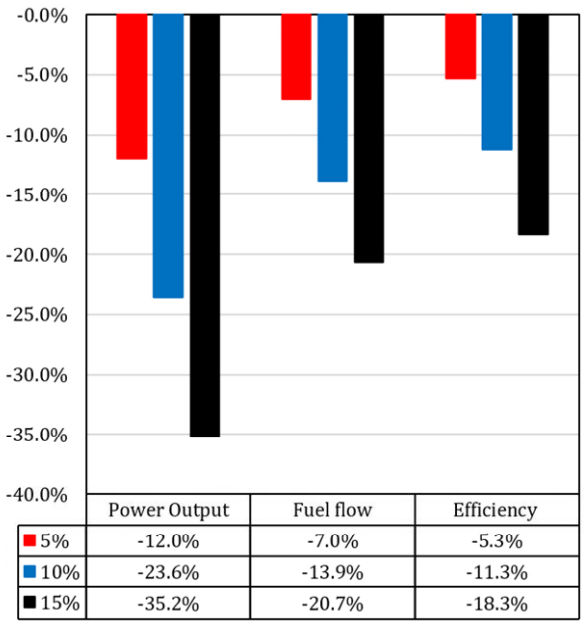

	Power Output	Fuel flow	Efficiency
5%	-12.0%	-7.0%	-5.3%
10%	-23.6%	-13.9%	-11.3%
15%	-35.2%	-20.7%	-18.3%

Figure 5: Effect of flow extractions on performance – max VIGV opening

The compressor characteristic map for comp.4 shown in **Figure 2**, is presented in **Figure 6,** highlighting the changes with flow extraction. It is important to note that the DP operating speed is 1 (100%) and the reason why this operating point does not coincide on the 1.01 corrected speed line. This compressor section has been selected as a result of the proximity to the station of air extraction. **Figure 6** shows that with increasing flow extraction, the operating points move towards choke that occurs at lower OPR and TET. It is noticeable that the operating point moves away from the surge line, thereby reducing the SMU as described by **Equation 8**. Towards choke, the inlet mass flow increases as shown from the operating points (DP to 15%). It is caused by reduced turbine work and less backpressure on the compressor. A similar effect also occurs in the early stages/compressors but to a lesser magnitude. The isentropic efficiency of comp. 4 changes with higher extraction as shown. At 5% and 10% extractions there is little or no change; this is determined by the shape (characteristics) of the map. Further extraction (at 15%) shows a marked reduction in the parameter.

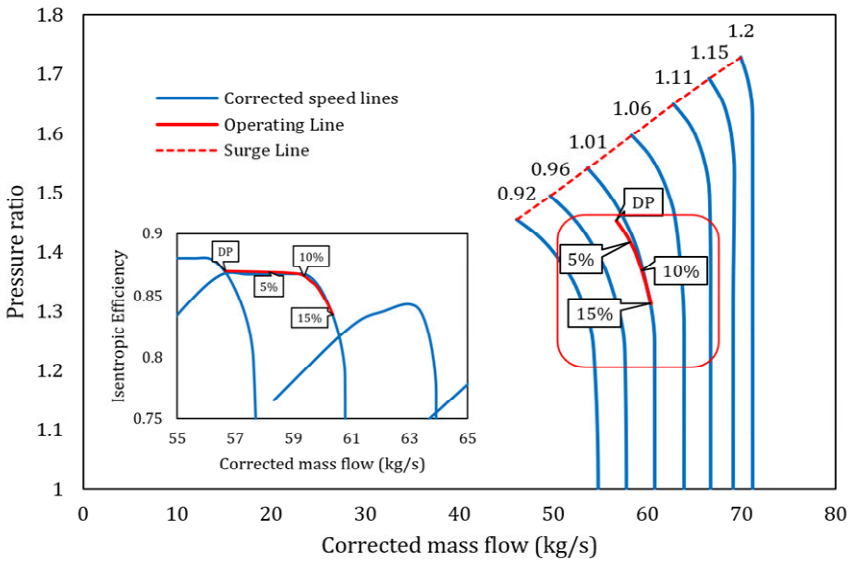

Figure 6: Operating points of comp. 4 with flow extractions

6. DESIGN MEL

In this section, the design or rated MEL of the engine is determined. As shown in

Figure *3*B, this is achieved by modulating the VIGV to its maximum closure at constant CMT in the first phase. It is important to note that the VIGV closure is limited by EGT that increases with the closure. Munoz de Escalona et al. [42] indicates that the EGT is allowed to increase up to 5% and suitable for CCGT operations. Nevertheless, the rise in EGT is not obtained in this operation due to the transition piece bypass cooling, as discussed previously. The second phase of turndown shown in

Figure *3*B indicates that only the CMT is reduced; this is until the limit to CO in **Table 1** is reached.

Figure 7 confirms the implications of the VIGIV closure on the characteristic behaviour in the front and back compressor, where 0° is the maximum opening and 40° is the maximum closing position. It

is shown that the comp. 1 is rescaled and tends towards the left of the map to a lower pressure ratio and CMF. For the back comp. 4, the map remains unchanged, however, the operating point shifts towards the right-hand side of the map to higher pressure ratio and CMF. This is caused by a higher drop in inlet pressure than the corresponding drop in flow and temperature, respectively. With the increase in pressure ratio at the back compressor, the SMU increases, while for the front compressor it is a reduction in the SMU as it becomes unloaded. **Figure 8** shows a complete view of the strategy for the operation, that includes phase 2 on the left of the figure. This shows the drop in power output for both phases; at the end of VIGV closure, it is 68% of the DP, while at the end of the drop in CMT it is 45% of DP. It also indicates that reductions in the parameters are more drastic in the first phase than in the latter.

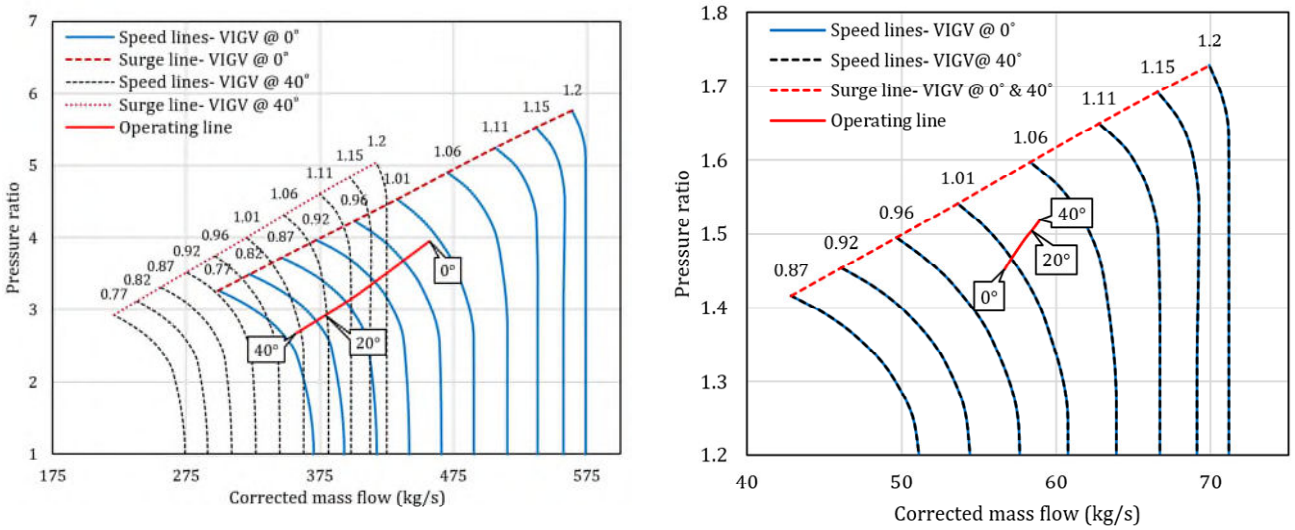

comp. 1 **comp. 4**

Figure 7: Front and back compressor maps at the max opening of VIGV – phase 1

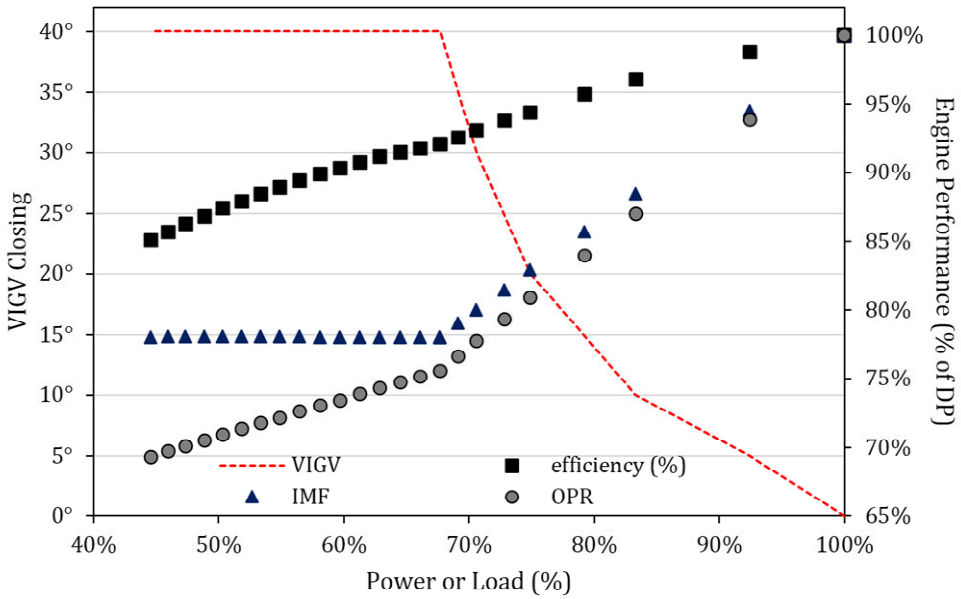

Figure 8: Variation of performance parameters – phase 1 and 2

The changes in the temperatures associated with the combustor in both phases are shown in **Figure 9**. They show similar trends but differ in the magnitude of change. The TET drop is influenced by a decreasing cooling flow temperature, at lower power outputs, though the cooling flow increases. The EGT drop is directly influenced by the reduced turbine flow expansion. For the flame temperature shown on the right of the figure, based on **Equation 9**, the plot is similar. An approximate temperature difference between the flame and CMT of 123 K is calculated for the turndown process.

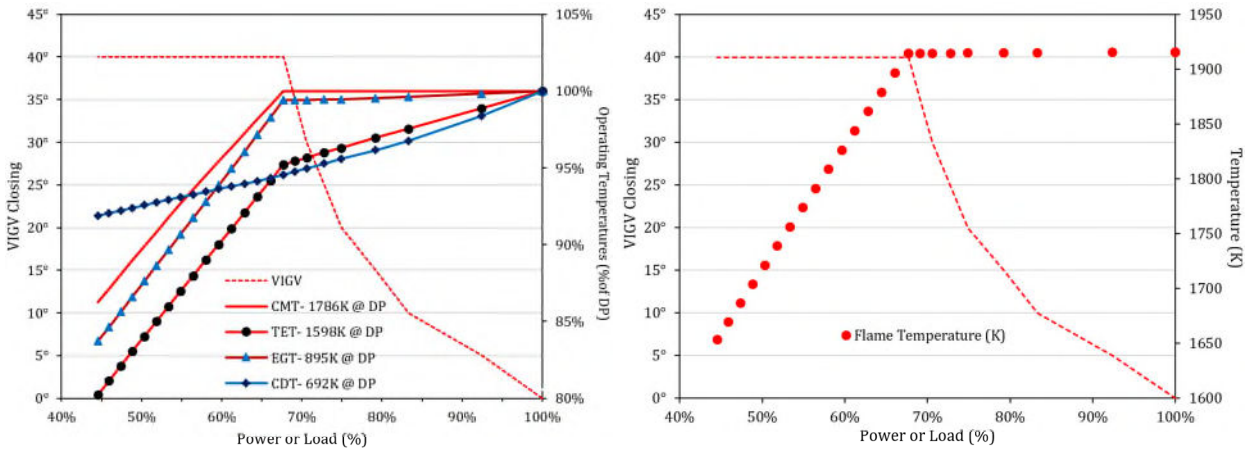

A. Engine model temperatures **B.** Emission model temperature

Figure 9: Variation of temperatures – phase 1 and 2

To attain the MEL, the corresponding NO_x and CO emissions were calculated based on Section 3, for both phases. The estimated NO_x emission is mostly impacted by the fuel-air ratio, combustor inlet mass flow and temperature as can be observed from **Equation 11.** These parameters decrease when the engine is turned down to lower loads and contribute to the drop in the NO_x emission. On **Figure 10,** a gradual slope is observed for NO_x values during VIGV closing; it becomes steeper as the CMT is reduced (phase 2). Furthermore, this trend conforms to the general theory that reduced flame temperatures inhibit NO_x production. On the other hand, CO emissions are seen to increase exponentially across the turndown. The exponential nature of the curve suggests that the emission is most sensitive to flame temperature variations. Like NO_x, the reduction in OPR leading to a lower combustor inlet pressure, compliments the flame temperature effect by further reducing the reaction rate. This results in incomplete combustion which fosters the production of CO. The figure also shows an intersection of the estimated CO emission curve with the CO limit (40.5 ppm) as indicated in **Table 1**. This point is the DP MEL, achieved at **47%** of the engine's PO.

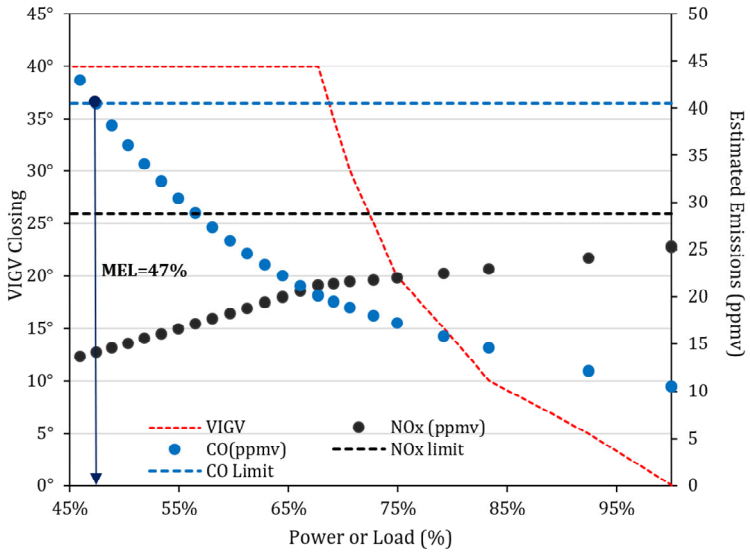

Figure 10: Variation of CO and NOx – phase 1 and 2

7. MEL EXTENSION

The new MEL (E-MEL) presented here and shown in

Figure *3*C is achieved through the VIGV full closure in phase 1, followed by the extraction of airflow from the compressor discharge in phase 2. Unlike the design case, the CMT is maintained for both phases (and not just the first). The aim here is to obtain the same levels of CO emissions as in the design case, at lower power output. Continuously keeping CMT fixed, with further reductions of mass flow in the engine, is seen to slow the inevitable rate of rise in CO at low loads, as shown subsequently.

Figure 11 shows phase 1 (right-hand side) that is identical to the design case. Phase 2 shows discrete extractions that drops the OPR less significantly for a given power when compared to the design case in **Figure 8.** This also infers a higher combustor inlet pressure - P_{13} than the corresponding power for the design case. From **Equation 10,** it can be deduced that higher P_{13} with the numerator being constant, amounts to a lower value of CO. The temperature variations in this operation are shown in **Figure 12,** also indicating generally higher values than in **Figure 9** at phase 2. For the same comparative power output with the design case, it can also be deduced that the EGT here is greater, and the flame temperature is almost unchanged. The negligible decline in flame temperature (observed below 70% of power) is due to the reductions in combustion airflow properties; which is compensated by increments in fuel-air ratio to maintain the CMT.

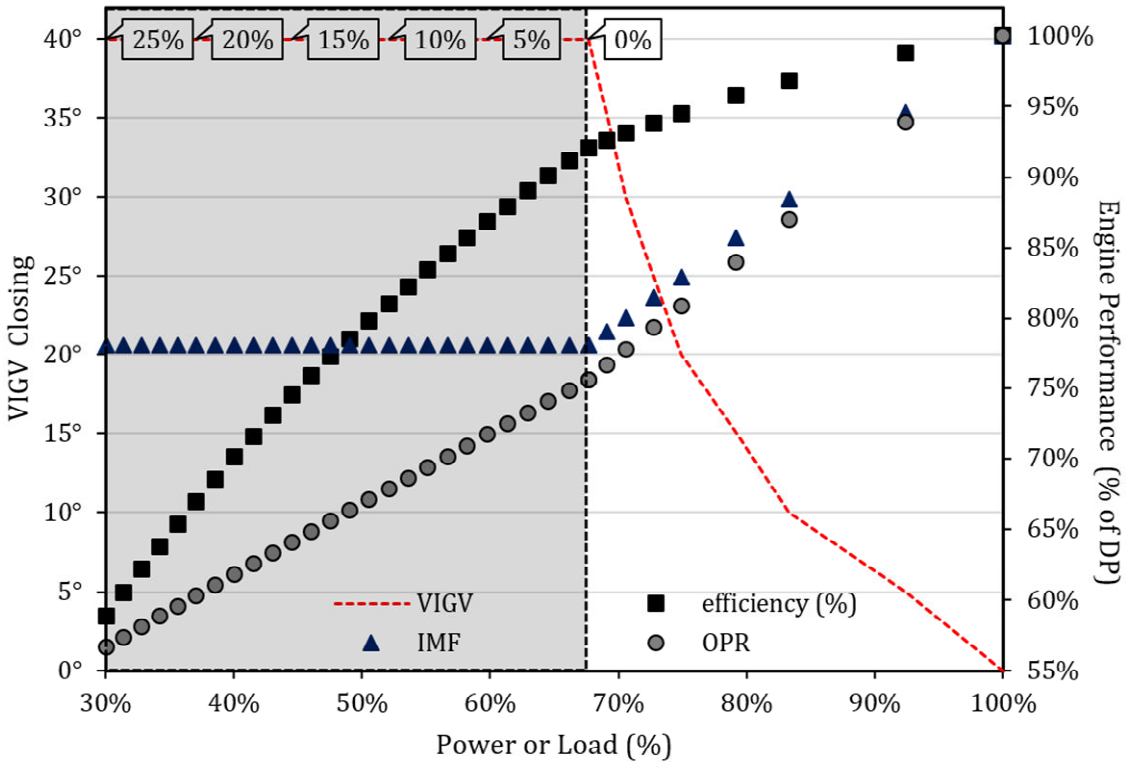

Figure 11: E-MEL: variation of performance parameters – phase 1 and 2

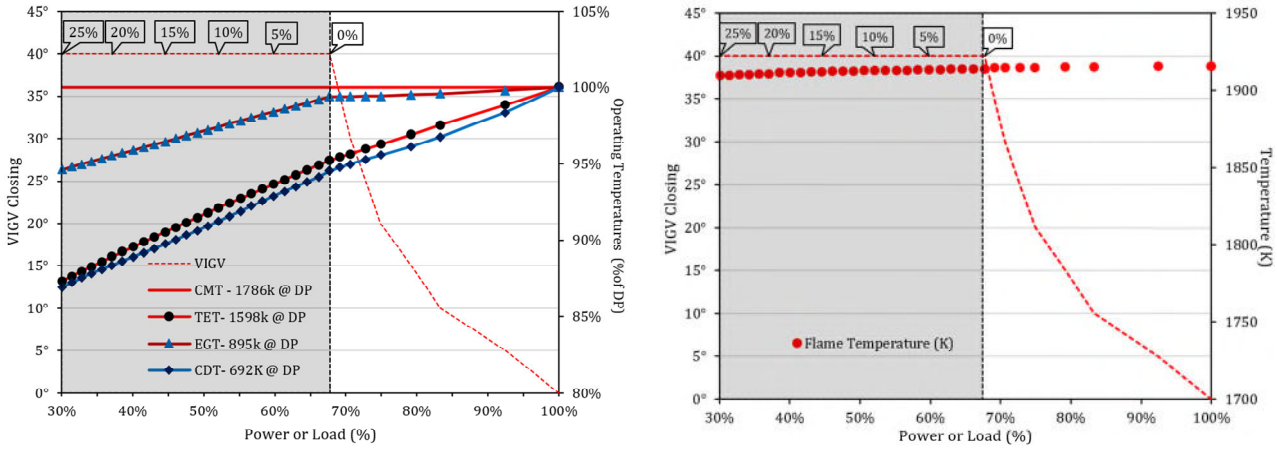

A. Engine model temperatures **B.** Emission model temperature

Figure 12: E-MEL: variation of temperatures – phase 1 and 2

For the emissions (CO and NO_x) calculated, it can be observed from **Figure 13**, that 40.5 ppm of CO is achieved at lower power of 31% of the design. This signifies an improvement in MEL from 47% and indicates a 34% reduction. The figure also shows that if the design MEL (47%) is to be maintained, CO emissions will be reduced by about 10 ppm with 14% of air extraction. The E-MEL occurs at 24% extraction of the compressor discharge flow, which is 20% of the compressor inlet airflow. However, it is important to reiterate that the back of the compressor (comp.4) still operates satisfactorily in this condition.

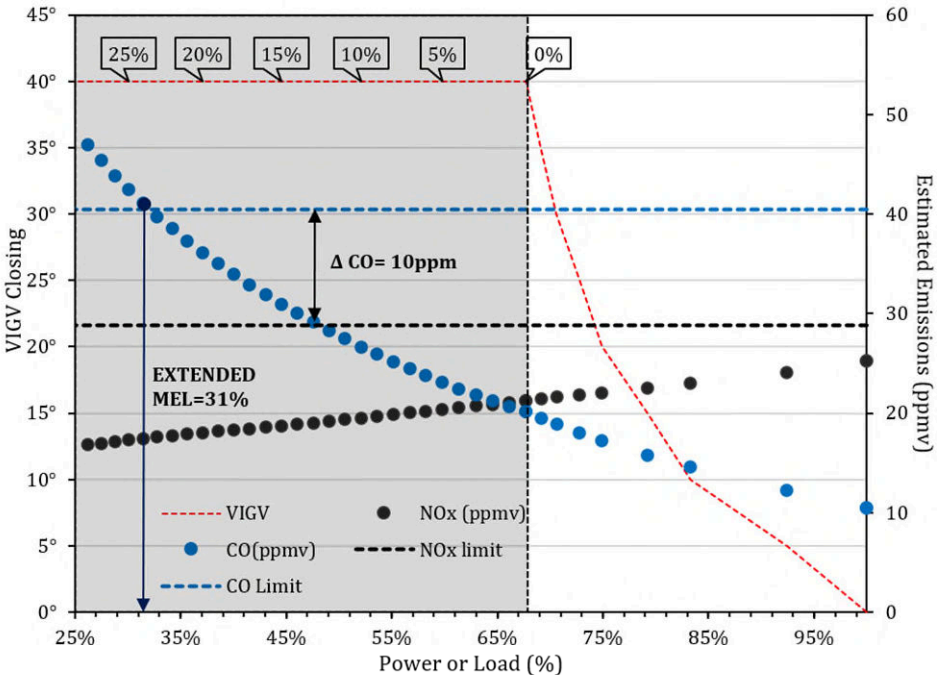

Figure 13: E-MEL: variation of CO and NOx – phase 1 and 2

The influence of ambient temperature on MEL extension is shown in **Figure 14**. The figure shows a higher capacity to improve MEL at lower ambient temperatures that are associated with higher OPR (due to increased air density). This results in higher combustor inlet pressure, P_{13} that brings about a lower CO for the same T_{flame} or CMT as explained. Hence, higher ambient temperatures are shown to reduce the MEL extension. The figure also illustrates the extraction quantities required to achieve the MEL extension. At lower ambient temperatures, higher percentages of airflow are extracted in comparison to higher temperatures. This suggests a higher potential for more storage at cold temperatures, though, at the expense of lower CDT (also extraction temperature) that is important for energy storage. The figure highlights the trade-off between flow quantity and temperature during extraction. It is worth mentioning that there is only a small variation in the design MEL at different ambient temperatures and not included in **Figure 14**.

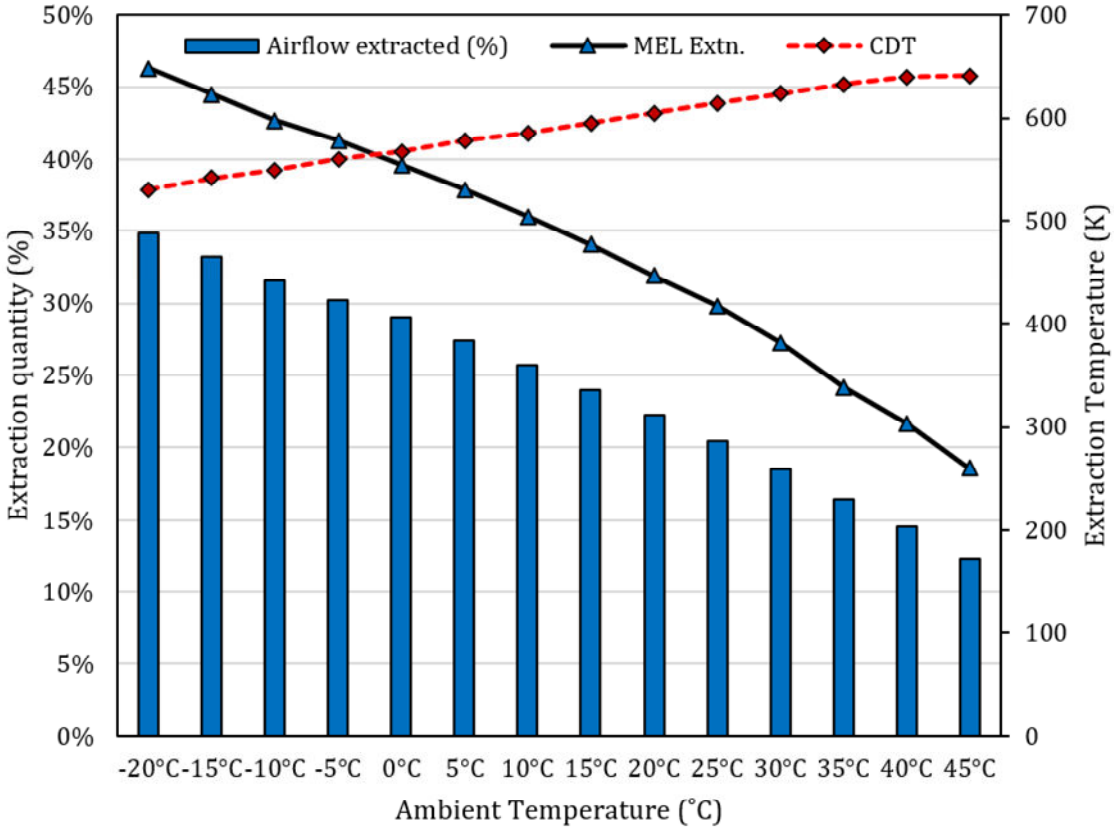

Figure 14: Influence of ambient temperatures on MEL extension

Following, the case presented in

Figure *3*C, another variant of MEL extension is considered. It includes a drop in the CMT in phase 2 (following VIGV closure and air extraction) as shown in **Figure 15**, for different cases of air extractions. As expected, the highest extraction leads to the biggest drop in power. It also indicates that lower MEL is achieved with more extractions at higher CMT. This will not be the case if the same amount of extraction is maintained with a lower CMT, as a reduction in T_{flame} will decrease P_{13} more adversely. **Equation 10** shows an exponential operator on temperature that will amount to a larger numerator when T_{flame} is reduced. This confirms that maintaining the design CMT throughout the operation (as in **Figure 12**) is the most favourable. At 20% extraction here, the corresponding new MEL of 35% is at a lower CMT, with a drop of 33 K. Though not the optimal in comparison to the 31% MEL obtained at fixed CMT and 24% air extraction, it brings about a substantive reduction in operating temperature that can extend the life of the combustor.

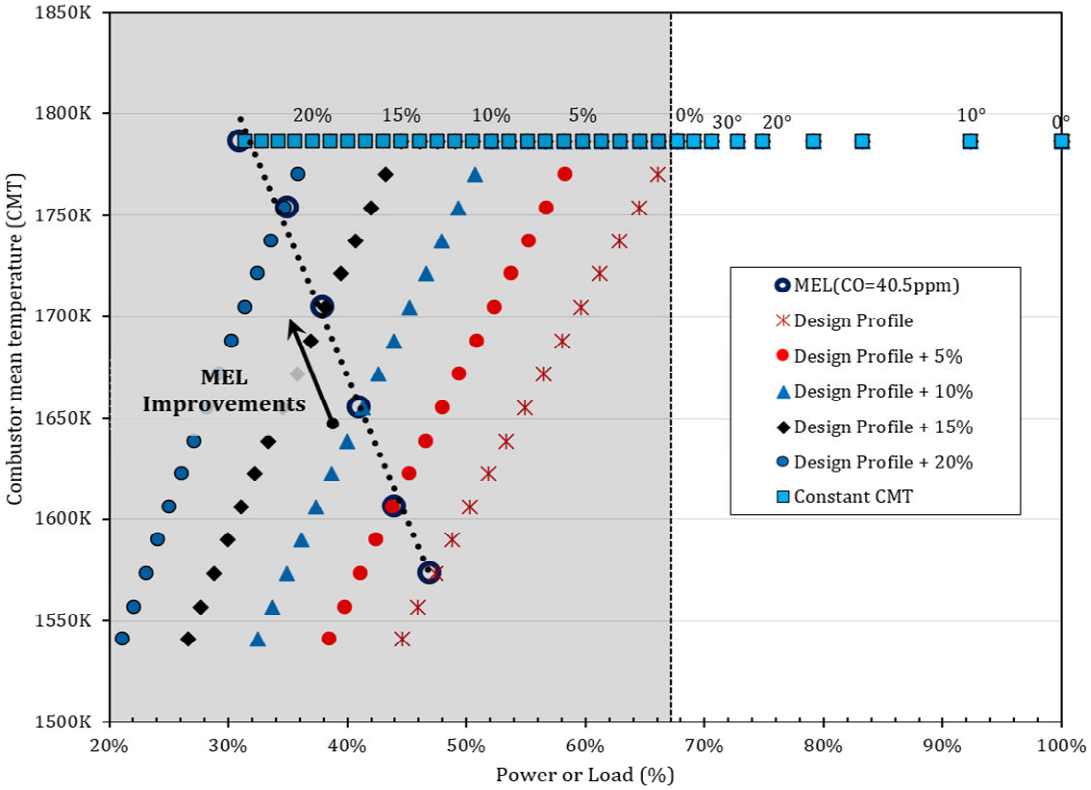

Figure 15: Alternative approach to MEL extension

8. CONCLUSIONS

The study has investigated the potentials to improve the minimum environmental load (MEL) of a stand-alone gas turbine engine. An MEL extension of 34% was achieved with 24% of flow extraction. This is possible when the regime includes constant combustor mean temperature (CMT) and variable inlet guide vane (VIGV) closure. The analysis shows that airflow extraction at the back of the compressor will:

- reduce the rate of CO rise when conducted immediately following VIGV closure and at a constant CMT, hence improve the MEL. This is achieved with a relatively smaller drop in combustor inlet pressure, in relation to the mass flow decrease.
- improve the MEL at lower ambient temperature at the expense of lower compressor discharge temperature (CDT) and hence less heat for storage.
- lead to choking of compressor stages nearest to the extraction location, at higher values of extractions
- reduce the overall pressure ratio (OPR), CDT, power output (PO) and thermal efficiency

Two strategies were implemented; one based on keeping CMT constant in all phases. While the second is by reducing the CMT after VIGV closure and air extractions. The former achieves an extended MEL

of 31%, whilst the latter shows less improvement in MEL. Nevertheless, the second case is beneficial for operational temperatures in the combustor that can improve lifing.

The corresponding amount of air extraction for the constant CMT operation is 24% of compressor discharge flow (20% with respect to the compressor inlet flow at part-load and 15.5% of full-load). However, the extracted quantity is expected to vary slightly with different compressor design. Maintaining the same CMT means the temperatures are not unusual for combustor durability and lifing, although the flame stability is open to investigation. The flame temperature and emission correlations used are fair approximations in the absence of very detailed methods and some combustor descriptions. Uncertainties related to this is not likely to affect the analysis of the results and overall conclusions as far as changes in parameters are concerned. A significant amount of effort has been put into the modelling of the engine, also accounting for a cooling flow schedule into the combustor exit. The schedule is as a function of load, apart from other cooling that exists. These affect the off-design behaviour of the engine and outcomes.

Finally, this work shows effects of air extraction for compressed air energy storage (CAES) that differ from other turndown approaches, in the larger amount of air that can be extracted from the compressor, as well as the extraction position (compressor discharge), unlike extra closing of VIGV. The outcomes show how important it is to maintain the CMT, hence higher combustor inlet pressure, to achieve lower MEL with flow extractions.

ACKNOWLEDGEMENT

This study is part of TURBO-REFLEX project that has received funding from the European Union's Horizon 2020 research and innovation programme, under grant agreement No. 764545.

DATA ACCESS STATEMENT

Data underlying this study can be accessed through the Cranfield University repository at 10.17862/cranfield.rd.12809402

NOMENCLATURE

01 - 22	Location on Engine Schematic
BAT	Best Available Techniques
BOV	Blow Off Valves
BREF	BAT Reference Documents
CAES	Compressed Air Energy Storage
CCGT	Combined Cycle Gas Turbine
CDT	Compressor Discharge Temperature, K
CDP	Compressor Discharge Pressure, bar

CMF	Corrected Mass Flow, kg/s
CMT	Combustor Mean Temperature, K
CO	Carbon Monoxide
COT	Combustor Outlet Temperature, K
DP	Design Point
EGT	Exhaust Gas Temperature, K
GT	Gas Turbine
IMF	Inlet Mass Flow, kg/s
ISO	International Organization for Standardization
$\dot{m}$	Mass Flow, kg/s
Max	Maximum
MEL	Minimum Environmental Load
N	Spool Speed (rpm)
NOx	Nitrous Oxides
OCGT	Open Cycle Gas Turbine
OEM	Original Engine manufacturers
OPR	Overall Pressure Ratio
P	Pressure, Pa
PO	Power Output, MW
PR	Pressure Ratio
SF	Scaling Factor
SMU	Surge Margin Utilisation
T	Temperature, K
TET	Turbine Entry Temperature, K
VIGV	Variable Inlet Guide Vanes

ψ	Hydrogen to Carbon atomic ratio of fuel
θ	Normalized fuel Temperature
π	Normalized fuel Pressure
τ	Residence time, s
η_{is}	Isentropic Efficiency

APPENDIX A

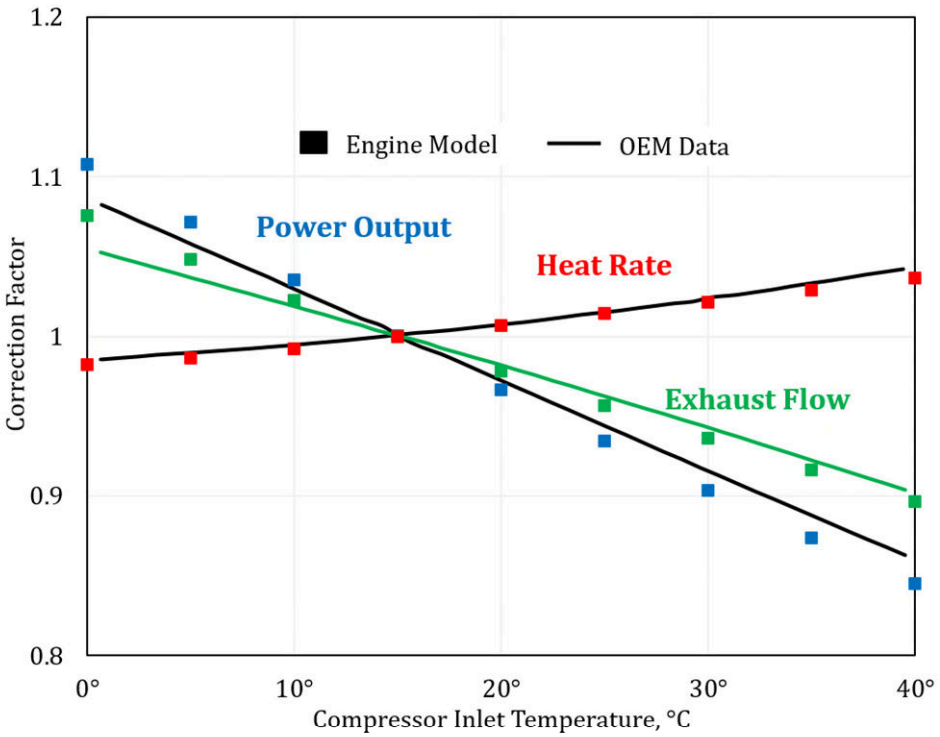

Figure A.1 Effect of inlet air temperature on the PO, heat rate and exhaust flow - model and reference engine

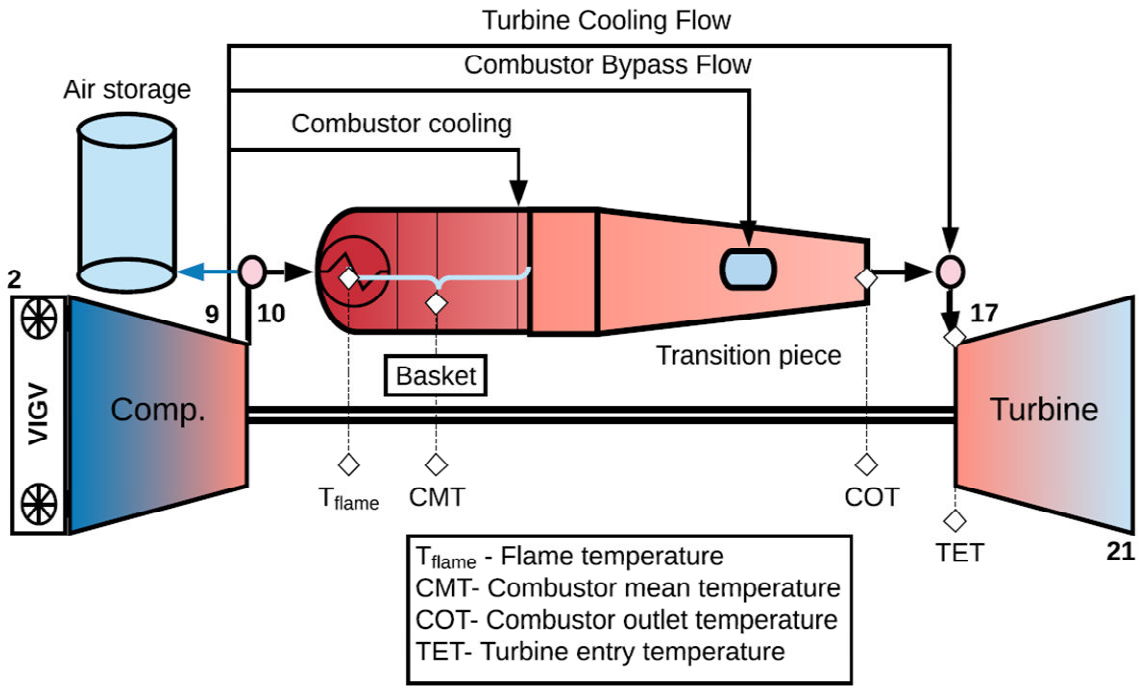

Figure A.2 Engine schematic with emphasis on combustion temperatures

Table A.1 Constants for Calculating Flame Temperature

	$0.92 \leq \theta < 2$	$2 \leq \theta < 3.2$
A	2361.764	2315.752
α	0.1157	-0.0493
β	-0.9489	-1.1141
λ	-1.0976	-1.1807
a_1	0.0143	0.0106
b_1	-0.0553	-0.045
c_1	0.0526	0.0482
a_2	0.3955	0.5688
b_2	-0.4417	-0.55
c_2	0.141	0.1319
a_3	0.0052	0.0108
b_3	-0.1289	-0.1291
c_3	0.082	0.0848

REFERENCES

[1] M. A. Gonzalez-Salazar, T. Kirstena and L. Prchlikb, "Review of the operational flexibility and emissions of gas- and coal-fired power plants in a future with growing renewables," *Renewable and Sustainable Energy Reviews,* vol. 82, no. 1, pp. 1497-1513, February 2018.

[2] J. E. Bisline, "Turn Down for What? The Economic Value of Operational Flexibility in Electricity Markets," *IEEE Transactions for Power Systems,* vol. 34, no. 1, pp. 527-534, January 2019.

[3] T. Lecomte, J. F. F. d. l. Fuente, F. Neuwahl, M. Canova, A. Pinasseau, I. Jankov, T. Brinkmann, S. Roudier and L. D. Sancho, "Best Available Techniques (BAT) Reference Documents for Large Combustion Plants," European Commission, Luxembourg, 2017.

[4] Siemens, "Turn Down," 2019. [Online]. Available: https://new.siemens.com/global/en/products/energy/services/performance-enhancement/modernization-upgrades/gas-turbines/turn-down-sgt-4000f.html. [Accessed 11 June 2019].

[5] M. Cioffi, S. Piola, E. Puppo, A. Silingardi and F. Bonzani, "Minimum Environmental Load Reduction in Heavy Duty Gas Turbines by Bleeding Lines," in *ASME Turbo Expo 2014: Turbine Technocal Conference and Exposition*, Dusseldorf, 2014.

[6] N. Pratyush, L. David, P. Adam and R. Douglas, "Low Load Operational Flexibility for Siemens F- and G-Class Gas Turbines," in *ASME Turbo Expo 2010: Power for Land, Sea, and Air*, Glasgow, 2010.

[7] C. Ruchti, H. Olia, K. Franitza, A. Ehrsam and W. Bauver, “Combined Cycle Power Plants as ideal solution to balance grid fluctuations Fast Start-up Capabilities,” in *Colloquium of Power PLant Technologies*, Dresden, 2011.

[8] F. Malavasi, P. Pesce, A. V. Pesenti, P. Traverso and D. Zito, “Ansaldo AE94.3A combustion improvement towards flexibility through extensive field testing,” in *ASME Turbo Expo 2013: Turbine Technical Conference and Exposition*, San Antonio, 2013.

[9] E. Deuker, M. H. Koenig, M. Moeller, J. Slad and H. Streb, “SGT5-4000F Gas Turbine and Combined Cycle Power Plant Evolution reflecting the changing Market Requirements,” in *PowerGen Europe*, Vienna, 2013.

[10] M. H. Baumgartner and T. Sattelmayer, “Improvement of the turn-down ratio of gas turbines by autothermal on board syngas generation,” *Journal of the Global Power and Propulsion Society,* vol. 1, pp. 55-70, 2017.

[11] J. D. Wojcik and J. Wang, “Feasibility study of Combined Cycle Gas Turbine (CCGT) power plant integration with Adiabatic Compressed Air Energy Storage (ACAES),” *Applied Energy,* vol. 221, pp. 477- 489, 2018.

[12] Parsons Brinckerhoff, “Technical Review of Innovative GTI-Storage System,” Parsons Brinckerhoff, Manchester, 2015.

[13] U. Igie, M. Abbondanza, A. Szymański and T. Nikolaidis, “Impact of Compressed Air Energy Storage Demands on Gas Turbine Performance,” *ASME Journal of Engineering for Gas Turbines and Power- Under Review,* 2019.

[14] R. Hackney, T. Nikolaidis and A. Pellegrini, “A method for modelling compressor bleed in gas turbine analysis software,” *Applied Thermal Engineering,* vol. 172, 25 May 2020.

[15] C. Yang, P. Wang, K. Fan and X. Ma, “Performance of gas turbine multi generation system regulated with compressor bypass extraction air energy storage,” *Applied Thermal Engineering,* vol. 172, 25 May 2020.

[16] Mitsubishi Hitachi Power Systems, “M501F Series,” Mitsubishi Hitachi Power Systems Global, [Online]. Available: https://www.mhps.com/products/gasturbines/lineup/m501f/index.html. [Accessed 7 February 2019].

[17] Mitsubishi Hitachi Power Systems (MHPS), “M501D,” [Online]. Available: https://www.mhps.com/products/gasturbines/lineup/m501d/index.html. [Accessed 18 April 2020].

[18] Mitsubishi Hitachi Power Systems (MHPS), “M701D,” [Online]. Available: https://www.mhps.com/products/gasturbines/lineup/m701d/index.html. [Accessed 18 April 2020].

[19] Mitsubishi Hitachi Power Systems (MHPS), “M701G,” [Online]. Available: https://www.mhps.com/products/gasturbines/lineup/m701g/index.html. [Accessed 18 April 2020].

[20] Mitsubishi Hitachi Power Systems (MHPS), “M501G,” [Online]. Available: https://www.mhps.com/products/gasturbines/lineup/m501g/index.html. [Accessed 18 April 2020].

[21] Mitsubishi Hitachi Power Systems (MHPS), “M501J,” [Online]. Available: https://www.mhps.com/products/gasturbines/lineup/m501j/index.html. [Accessed 18 April 2020].

[22] Mitsubishi Hitachi Power Systems (MHPS), “M701F,” [Online]. Available: https://www.mhps.com/products/gasturbines/lineup/m701f/index.html . [Accessed 18 April 2020].

[23] GE, “GE 7F,” [Online]. Available: https://www.ge.com/content/dam/gepower-pgdp/global/en_US/documents/product/gas%20turbines/Fact%20Sheet/2017-prod-specs/7f-power-plants.pdf. [Accessed 18 April 2020].

[24] GE, “GE 9E,” [Online]. Available: https://www.ge.com/content/dam/gepower-pgdp/global/en_US/documents/product/gas%20turbines/Fact%20Sheet/2017-prod-specs/GEA32931A%209E-GT13E2_Power_Plants_R2.pdf. [Accessed 18 April 2020].

[25] GE, “GE 7E,” [Online]. Available: https://www.ge.com/content/dam/gepower-pgdp/global/en_US/documents/product/gas%20turbines/Fact%20Sheet/2017-prod-specs/GEA32932A%207E_Power_Plants_R1.pdf. [Accessed 18 April 2020].

[26] GE, “GE 6F,” [Online]. Available: https://www.ge.com/content/dam/gepower-pgdp/global/en_US/documents/product/gas%20turbines/Fact%20Sheet/2018-prod-specs/6F_Power_Plants_R2.pdf. [Accessed 18 April 2020].

[27] GE, “GE 9HA,” [Online]. Available: https://www.ge.com/content/dam/gepower-pgdp/global/en_US/documents/product/gas%20turbines/Fact%20Sheet/2017-prod-specs/9ha-power-plants.pdf. [Accessed 18 April 2020].

[28] Ansaldo Energia, “Anasaldo Energia A64.3A,” [Online]. Available: https://www.ansaldoenergia.com/PublishingImages/AE64.3A/A64.3A.pdf. [Accessed 18 April 2020].

[29] Ansaldo Energia, “Ansaldo Energia A94.3A,” [Online]. Available: https://www.ansaldoenergia.com/PublishingImages/AE94.3A/AE94.3A.pdf. [Accessed 18 April 2020].

[30] Ansaldo Energia , “Ansaldo Energia AE94.2,” [Online]. Available: https://www.ansaldoenergia.com/PublishingImages/AE94.2/AE94.2.pdf. [Accessed 18 April 2020].

[31] Ansaldo Energia, “Ansaldo Energia GT36,” [Online]. Available: https://www.ansaldoenergia.com/PublishingImages/GT36/GT36.pdf. [Accessed 18 April 2020].

[32] Ansaldo Energia , “Ansaldo Energia GT26,” [Online]. Available: https://www.ansaldoenergia.com/PublishingImages/GT26/GT26.pdf. [Accessed 18 April 2020].

[33] T. Nikolaidis, “The Turbomatch Scheme,” 2015.

[34] K. TANAKA, K. NISHIDA and W. AKIZUKI, “Gas Turbine Combustor Technology Contributing to Environmental Conservation,” *Mitsubishi Heavy Industries Technical Review,* vol. 46, no. 2, June 2009.

[35] P. P. Walsh and P. Fletcher, Gas Turbine Performance, 2nd ed., B. S. Limited, Ed., Oxford: Blackwell Science Limited, 2004.

[36] S. C. Gulen, “Modern gas Turbine Combined Cycle,” *Turbomachinery International,* no. November/December, 2013.

[37] O. Gulder, “Flame Temperature Estimation of Conventional and Future Jet Fuels,” *Journal of Engineering for Gas Turbines and Power,* vol. 108, no. 2, pp. 376-380, 1986.

[38] R. N. and M. H., “Emissions predictions of different gas turbine combustors,” in *32nd Aerospace Sciences Meeting & Exhibit*, Reno, 1994.

[39] S. Etemad, “Industrial Gas Turbine Engine Catalytic Pilot Combustor -,” Precision Combustion, Inc., North Haven, 2010.

[40] A. H. Lefebvre and D. R. Ballal, Gas Turbine Combustion: Alternative Fuels and Emissions, Boca Raton, Florida: Taylor & Francis Group, LLC, 2010, pp. 153-154.

[41] D. A. Sullivan, “A Simple Gas Turbine Combustor NOx Correlation Including the Effect of Vitiated Air,” *Journal of Engineering for Power,* vol. 99, no. 2, pp. 145-152, 1977.

[42] J. M. d. Escalona, D. Sánchez, R. Chacartegui and T. Sánchez, “Part-load analysis of gas turbine & ORC combined cycles,” *Applied Thermal Engineering,* vol. 36, pp. 63 - 72, April 2012.

[43] D. Therkorn, M. Gassner, V. Lonneux, M. Zhang and S. Bernero, “CCPP Operational Flexibility Extension Below 30% Load Using Reheat Burner Switch-Off Concept,” in *ASME Turbo Expo 2015: Turbine Technical Conference and Exposition*, Montreal, 2015.

2020-08-14

Gas turbine minimum environmental load extension with compressed air extraction for storage

Abudu, Kamal

Elsevier

Abudu K, Igie U, Minervino O, Hamilton R. (2020) Gas turbine minimum environmental load extension with compressed air extraction for storage. Applied Thermal Engineering, Volume 180, November 2020, Article number 115869

https://doi.org/10.1016/j.applthermaleng.2020.115869